Sol–Gel and Isotropic/Nematic Transitions in Aqueous Suspensions of Natural Nontronite Clay. Influence of Particle Anisotropy. 2. Gel Structure and Mechanical Properties

ARTICLE *in* LANGMUIR · JANUARY 2009

Impact Factor: 4.46 · DOI: 10.1021/la801894a · Source: PubMed

8 AUTHORS, INCLUDING:

Laurent J Michot
French National Centre for Scientific Resea…
160 PUBLICATIONS **3,281** CITATIONS
SEE PROFILE

Isabelle Bihannic
French National Centre for Scientific Resea…
50 PUBLICATIONS **995** CITATIONS
SEE PROFILE

Pierre Emile Levitz
Pierre and Marie Curie University - Paris 6
190 PUBLICATIONS **5,450** CITATIONS
SEE PROFILE

Patrick Davidson
Université Paris-Sud 11
176 PUBLICATIONS **4,504** CITATIONS
SEE PROFILE

Sol−Gel and Isotropic/Nematic Transitions in Aqueous Suspensions of Natural Nontronite Clay. Influence of Particle Anisotropy. 2. Gel Structure and Mechanical Properties

Laurent J. Michot,*[,†] Christophe Baravian,*[,‡] Isabelle Bihannic,[†] Solange Maddi,[†] Christian Moyne,[‡] Jérôme F. L. Duval,[†] Pierre Levitz,[§] and Patrick Davidson[||]

Laboratoire Environnement et Minéralurgie, Nancy University, CNRS-INPL UMR 7569 BP40 54501 Vandaeuvre Cedex, France, Laboratoire d'Energétique et de Mécanique Théorique et Appliquée, Nancy University, UMR 7563 CNRS-INPL-UHP, 2, Avenue de la Forêt de Haye, BP160 54504 Vandaeuvre Cedex, France, Laboratoire de Physique de la Matière Condensée, Polytechnique Ecole Polytechnique, UMR 7643 CNRS, 91128 Palaiseau Cedex, France, and Laboratoire de Physique des Solides, Université Paris-Sud, UMR 8502 CNRS, Bât 510 91405 Orsay Cedex, France

Received June 16, 2008. Revised Manuscript Received October 13, 2008

After size-selection, the phase behavior of aqueous suspensions of nontronite clay was analyzed by osmotic pressure measurements, rheological experiments, and small-angle X-ray scattering. All the measurements confirm that for ionic strength $\leq 10^{-3}$ M/L, the system is purely repulsive. By combining results from osmotic pressure measurements and X-ray scattering, it appears that the pressure of the system can be well-described using a simple Poisson−Boltzmann treatment based on the interaction between charged infinite parallel planes. In terms of rheological properties, even if the status of the sol/gel transition remains partially unclear as the number density of particles at the sol−gel transition exhibits a −2 power dependence with average particle size, the yield stress and elasticity of the gels can be easily renormalized for all particle sizes on the basis of the volume of the particles. Furthermore, rheological modeling of the flow curves shows that for all the particles, an approach based on excluded volume effects captures most features of nontronite suspensions. Still, the high shear flow properties of the suspensions that reveal a strong orientation of particles in the flow are affected by electrostatic interactions. This study then shows that the rich phase behavior of clay minerals, notably the fact that some clay minerals display an isotropic/nematic transition while others exhibit a sol−gel transition, requires a full understanding of all the interactions in the system that can only be achieved by working on well-characterized size-selected samples.

Introduction

One of the most important properties of swelling clay minerals is their ability to form yield stress materials when dispersed in water. This feature, extensively used in various industrial applications (drilling fluids, food industry, cosmetic industry, etc.),[1,2] also plays a major role in many fundamental processes occurring at the Earth's surface, such as slipping processes in plate-boundary faults (e.g., ref 3) or landslide triggering (e.g., ref 4). For these reasons, numerous studies have focused on the rheology of aqueous clay suspensions. The rheological features of the suspensions in terms of yield stress, viscoelasticity, and thixotropy have been interpreted by two conflicting models, the so-called "house of cards" model[5,6] that assumes attractive interactions between faces and edges of the platelets and a model based on the formation of an oriented network stabilized by repulsive forces caused by interacting double layers.[7−9] Rheological interpretations favoring attractive interactions were provided in various works,[10−12] whereas numerous other works supported the second model to understand both gel structure and rheological properties.[13−21] However, except for a remarkable study carried out in 1937, by Hauser and Reed,[7] who worked on size fractionated Wyoming montmorillonites at high ionic strength, very few studies have analyzed the influence of particle size on the rheological properties of swelling clays. We recently carried out an analysis of the phase behavior of size-fractionated Wyoming montmorillonite[22] and showed that the sol−gel transition exhibited a nontrivial behavior with increasing particle anisotropy; i.e., higher particle size retarded the sol−gel transition. In addition, as far as the phase behavior of swelling clay minerals is concerned, significant differences can be observed depending

* Corresponding authors. E-mail: Laurent.michot@ensg.inpl-nancy.fr (L.J.M.), Christophe.baravian@ensem.inpl-nancy.fr (C.B.).
† Laboratoire Environnement et Minéralurgie, Nancy University.
‡ Laboratoire d'Energétique et de Mécanique Théorique et Appliquée, Nancy University.
§ Polytechnique Ecole Polytechnique.
|| Université Paris-Sud.

(1) Harvey, C. C.; Lagaly, G. In *Handbook of Clay Science*; Bergaya, F., Theng, B. G., Lagaly, G., Eds.; Elsevier: New York, 2006; Chapter 10.1.
(2) Maitland, G. C. *Proceedings of the Xth International Congress of Rheology*; Elsevier Science Publishers: Brussels, 1992; p 140.
(3) Saffer, D. M.; Frye, K. M.; Marone, C.; Mair, K. *Geophys. Res. Lett.* **2001**, *28*, 2297.
(4) Wan, Y. S.; Kwong, J. *Eng. Geol.* **2002**, *65*, 293.
(5) Broughton, G.; Squires, L. *J. Phys. Chem.* **1936**, *40*, 1041.
(6) Van Olphen, H. *Discuss. Faraday Soc.* **1951**, *11*, 82.
(7) Hauser, E. A.; Reed, C. E. *J. Phys. Chem.* **1937**, *41*, 911.
(8) Hauser, E. A. *Chem. Rev.* **1945**, *40*, 287.
(9) Norrish, K. *Discuss. Faraday Soc.* **1954**, *18*, 120.
(10) Van Olphen, H. *J. Colloid Interface Sci.* **1964**, *19*, 313.
(11) Khandal, R. K.; Tadros, Th. F. *J. Colloid Interface Sci.* **1988**, *125*, 122.
(12) Miano, F.; Rabaioli, M. R. *Colloids Surf. A* **1994**, *84*, 229.
(13) Weiss, A.; Frank, R. *Naturforsch* **1961**, *16*, 141.
(14) Callaghan, I. C.; Ottewill, R. *Faraday Discuss. Chem. Soc.* **1974**, *57*, 110.
(15) Rand, B.; Penkenc, E.; Goodwin, J. W.; Smith, R. W. *J. Chem. Soc. Faraday Trans.* **1980**, *76*, 225.
(16) Ramsay, J. D. F. *J. Colloid Interface Sci.* **1986**, *109*, 441.
(17) Vali, H.; Bachmann, L. *J. Colloid Interface Sci.* **1988**, *126*, 278.
(18) Lagaly, G. *Appl. Clay Sci.* **1989**, *4*, 105.
(19) Bradenburg, U.; Lagaly, G. *Appl. Clay Sci.* **1988**, *3*, 263.
(20) Abend, S.; Lagaly, G. *Appl. Clay Sci.* **2000**, *16*, 201.
(21) Ten Brinke, A. J. W.; Bailey, L.; Lekkerkerker, H. N. W.; Maitland, G. C. *Soft Matter* **2007**, 1145.
(22) Michot, L. J.; Bihannic, I.; Porsch, K.; Maddi, S.; Baravian, C.; Mougel, J.; Levitz, P. *Langmuir* **2004**, *20*, 10829.

10.1021/la801894a CCC: $40.75
Published on Web 12/09/2008

Table 1. Morphological Parameters of the Various Nontronite Size Fractions Deduced from the Analysis of the TEM Micrographs

size	minimal length (nm)	maximal length (nm)	average length (nm)	polydispersity length (%)	minimal width (nm)	maximal width (nm)	average width (nm)	polydispersity width (%)	average anisotropy in the plane
S1	239	2200	705	52	45	351	138	46	5.5
S2	112	986	368	41	45	245	93	39	4.2
S23	112	600	250	25	45	130	65	25	3.8
S3	53	345	147	39	20	120	52	37	3.1
S4	47	250	120	35	21	106	44	35	2.9

on the mineral used. Whereas synthetic hectorite (laponite), natural hectorite, and montmorillonite display a transition from liquid to gel (e.g., refs 20−30), we recently showed[31,32] that a ferruginous beidellite, nontronite, exhibited a true isotropic/nematic (I/N) transition occurring at a lower concentration than that of the sol−gel transition. The evolution with size of this I/N transition displayed a logical behavior and its position in the phase diagrams was well-described by simple excluded volume effects[33] based on Onsager's initial approach.[34]

The aim of the present paper is to extend the analysis of the size dependence to the sol−gel transition and to the rheological behavior of the gels and to define if the existence of a true I/N transition affects the gel properties when compared to those of other swelling clay minerals or if the two phenomena are not coupled at all.[35,36] In addition by examining jointly the structure of the gels by small angle X-ray scattering experiments, we will try to analyze the respective roles of electrostatics and excluded volume effects on the behavior of nontronite suspensions.

Materials and Methods

The clay mineral used in this study is a nontronite from Southern Australia[37] that was purchased from the Source Clays Minerals repository at Purdue University. Nontronite is a naturally occurring swelling dioctahedral clay mineral related to the montmorillonite−beidellite series in which most aluminum atoms are replaced by iron(III) ions. Its structural formula[38] can be written as $(Si_{7.55}Al_{0.16}Fe_{0.29})(Al_{0.34}Fe_{3.54}Mg_{0.05})O_{20}(OH)_4Na_{0.72}$. Before use, the mineral was homoionized with Na^+ ions and purified. Four size fractions referred to as sizes 1−4 were then obtained by successive centrifugations (Table 1). Experimental details are provided elsewhere.[31] One additional size was obtained by eliminating the coarser particles from size 2. It will be referred to thereafter as size 23. In the following, the sizes will be referred to as S1, S2, S23, S3, and S4.

Osmotic pressure measurements were carried out using Visking dialysis tubes with a cutoff of 14 000 Da. Experimental details are provided elsewhere.[31]

Rheological measurements were carried out at 25 °C using an AR 2000 rheometer from TA instruments with a cone and plate geometry with a diameter of 20 mm, a truncature of 14 μm, and an angle of 0.30°. The elastic and viscous moduli G' and G'' were determined from oscillatory stress controlled measurements using frequencies between 0.02 and 10 Hz after a pre-equilibration stage of 5 min. In all cases, the stress amplitude used during the experiments was chosen in the linear regime. At the end of the oscillatory experiments, a preshearing stage of 1 min at a shear rate of 5000 s^{-1} was applied, after which flow curves were recorded under controlled shear rate from 0 to 5000 s^{-1} with a logarithmic step (10 points per decade). The full cycle of increasing and decreasing shear rates was performed in 15 min.

Small angle X-ray scattering (SAXS) experiments were carried out on beamlines A2 and BW4 at Hasylab, Hamburg, Germany. Experiments on beamline A2 were performed using a fixed wavelength of 0.15 nm and a sample to detector distance of 3 m, whereas beamline BW4 was operated at a wavelength of 0.138 nm and a sample to detector distance of 13 m. The samples were conditioned in cylindrical glass capillaries, in square glass capillaries, or in wet cells between two kapton sheets. Two dimensional scattering patterns were collected on a CCD camera and the curves of scattered intensity vs scattering vector modulus q ($q = 4\pi \sin \theta/\lambda$, where 2θ is the scattering angle and λ the wavelength) were obtained by an angular integration of the data. When anisotropic patterns were observed, the integration was carried out in the direction of maximum intensity of the anisotropic patterns.

Results

Structure of the Suspensions. The phase diagrams corresponding to the five size fractions investigated were already presented in part I of the present study.[31] For clarity reasons, it seems important to recall them in the second part (Figure 1), as they provide the basis for discussion. All the samples are isotropic liquids for low volume fractions and birefringent gels for high volume fractions and moderate ionic strength. At high ionic strength, flocculation is observed. In addition, for the three smallest size fractions, a biphasic region indicating the occurrence of an isotropic/nematic first-order transition is observed. For the two higher size fractions, such a transition is not experimentally observed as sedimentation occurs, thus hindering a clear observation of the transition that should, however, be present.

The structure of the suspensions in the various regions of the phase diagrams was analyzed by SAXS. As shown in part 1 of this series of papers,[31] diffuse scattering peaks arising from short-range positional order are observed in the whole phase diagram. Their position q_{max} in reciprocal space can be related to the average interparticle distance D by considering that $D \approx 2\pi/q$. The evolution of the thus calculated interparticle distances with volume fraction is presented in Figure 2 for the five size fractions of nontronite. Common features are observed for all size fractions and all ionic strengths. In the high volume fraction region of the diagram, the curves scale as ϕ^{-1}, indicating a local lamellar order of the clay platelets with a unidimensional swelling law. Such a law can be used to derive the thickness, t, of the individual scattering objects. The average values obtained for the five size fractions are 1.05, 0.76, 0.72, 0.66, and 0.52 nm for size fractions S1, S2, S23, S3, and S4, respectively. As discussed previously,[32]

(23) Mourchid, A.; Delville, A.; Lambard, J.; Lécolier, E.; Levitz, P. *Langmuir* **1995**, *11*, 1942.
(24) Gabriel, J.-C. P.; Sanchez, C.; Davidson, P. *J. Phys. Chem.* **1996**, *100*, 11139.
(25) Mourchid, A.; Lécolier, E.; Van Damme, H.; Levitz, P. *Langmuir* **1998**, *14*, 4718.
(26) Bonn, D.; Kellay, H.; Tanaka, H.; Wegdam, G.; Meunier, J. *Langmuir* **1999**, *15*, 7534.
(27) Knaebel, A.; Bellour, M.; Munch, J.-P.; Viasnoff, V.; Lequeux, F.; Harden, J. L. *Europhys. Lett.* **2000**, *52*, 73.
(28) Martin, C.; Pignon, F.; Magnin, A.; Piau, J.-M.; Cabane, B.; Lindner, P. *Phys Rev E.* **2002**, *66*, Art no. 021401.
(29) Mongondry, P.; Tassin, J. F.; Nicolai, T. *J. Colloid Interface Sci.* **2005**, *283*, 397.
(30) Ruzicka, B.; Zulian, L.; Ruocco, G. *Langmuir* **2006**, *22*, 1106.
(31) Michot, L. J.; Bihannic, I.; Maddi, S.; Funari, S. S.; Baravian, C.; Levitz, P.; Davidson, P. *Proc. Natl. Acad. Sci. U.S.A.* **2006**, *103*, 16101.
(32) Michot, L. J.; Bihannic, I.; Maddi, S.; Baravian, C.; Levitz, P.; Davidson, P. *Langmuir* **2008**, *24*, 3127.
(33) Bates, M. A.; Frenkel, D. *J. Chem. Phys.* **1999**, *110*, 6553.
(34) Onsager, L. *Ann. N.Y. Acad. Sci.* **1949**, *51*, 627.
(35) Van der Beek, D.; Lekkerkerker, H. N. W. *Europhys. Lett.* **2003**, *61*, 702.
(36) Van der Beek, D.; Lekkerkerker, H. N. W. *Langmuir* **2004**, *20*, 8582.
(37) Keeling, J. M.; Raven, M. D.; Gates, W. P. *Clays Clay Miner.* **2000**, *48*, 537.
(38) Gates, W. P.; Slade, P. G.; Manceau, A.; Lanson, B. *Clays Clay Miner.* **2002**, *50*, 223.

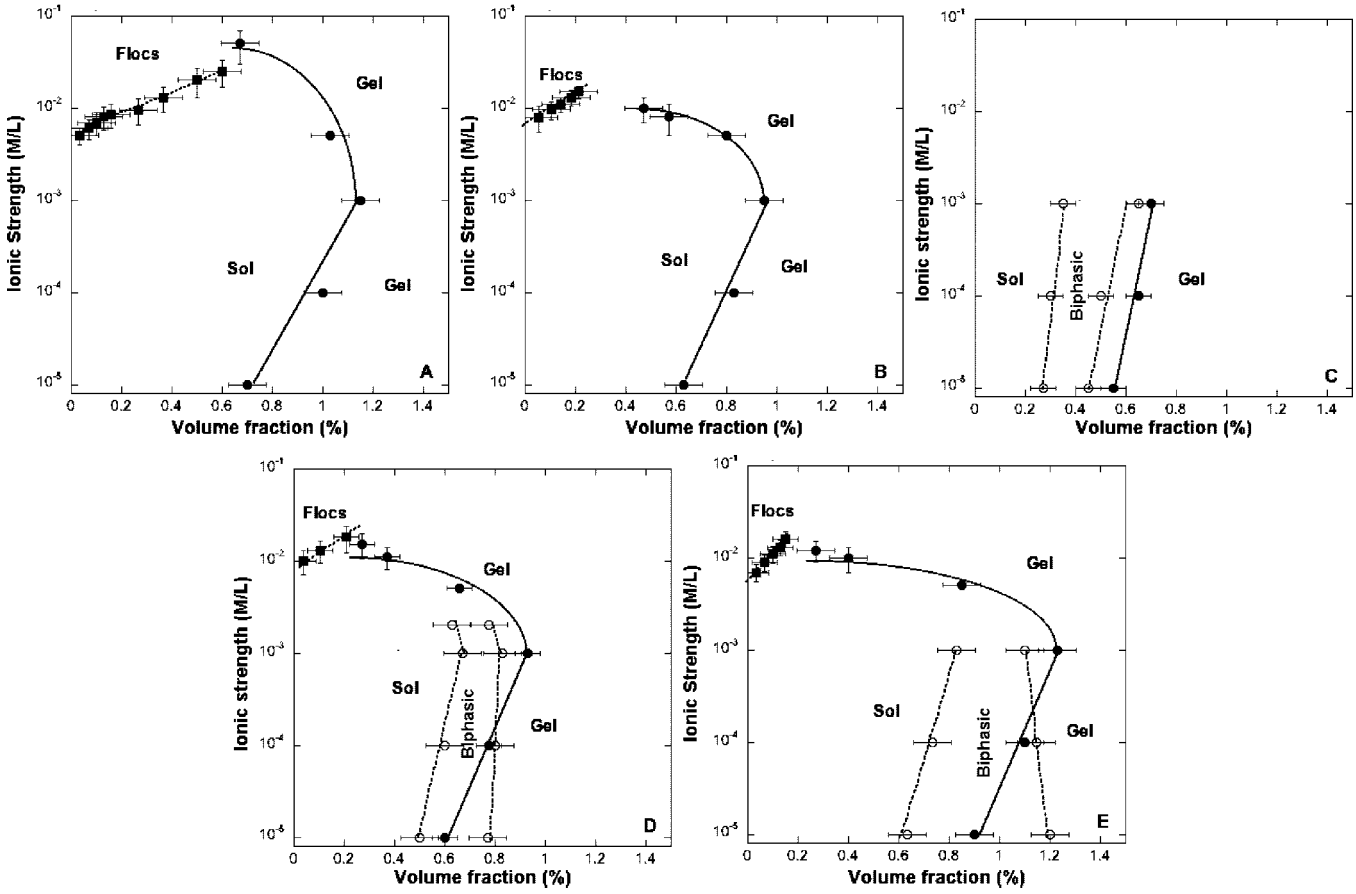

Figure 1. Phase diagrams of the five nontronite size fractions: A, S1; B, S2; C, S23; D, S3; E, S4.

such an evolution can be linked to a less perfect exfoliation of the larger size particles in aqueous solution. In the low volume fractions region, the curves display different evolutions depending on particle size. For the higher size fractions, the curves scale as $\phi^{-0.5}$, whereas for the two smaller size fractions, a regime where distances vary as $\phi^{-0.33}$ is observed. This latter regime can be assigned to isotropic volumic swelling. This regime could be reached at lower volume fractions for the more anisotropic particles (S1 and S2). However, such a regime could not be observed in the SAXS conditions used in the present study. It must be pointed out that the approximated formula according to which the interparticle distances were calculated does not have any influence on the features described above. A full rigorous treatment of the SAXS patterns based on an inverse Fourier transform to obtain pair distribution functions would lead to the same swelling laws.

Rheological Properties. Typical curves obtained from oscillatory stress measurements were presented in part 1 of the present series of papers.[32] For relatively high volume fractions, G' was much higher than G'' and exhibited a limited frequency dependence, typical of a gel behavior, whereas at lower volume fractions, the two moduli were on the same order of magnitude and the suspensions were then slightly viscous. As far as flow experiments are concerned, Figure 3 presents some typical curves obtained for the various size fractions of nontronite. For ionic strength $\leq 10^{-3}$ M/L (Figure 3A), the branches corresponding to increasing and decreasing shear rates are nearly superimposed, indicating that a steady-state is reached in these experiments.

Furthermore, contrary to rheological data recently presented on hectorite particles, another lath-shaped clay mineral,[21] except for very high volume fraction, the data do not reveal any significant shear-banding that would lead to significant hysteresis between the branches corresponding to increasing and decreasing flow rates. This difference may be due to various reasons. (i) In order to reach high shear rates (up to 5000 s^{-1}), the measurement geometry used in the present study was based on a very small angle with a truncature of 14 μm. (ii) Due to the size selection procedures used, the polydispersity of the particles is significantly reduced. (iii) Samples in the present study were prepared by osmotic stress starting from very dilute suspensions, thus ensuring a proper dispersion of the clay platelets. For an ionic strength of 5×10^{-3} M/L (Figure 3B), significant differences are observed at low shear rates between the ascending and descending ramps. These differences can be assigned to retarded viscoelasticity, which confirms, as already suggested by the phase diagrams (Figure 1) and by osmotic stress measurements,[32] that for such an ionic strength, phenomena such as microflocculation occur and modify the rheology of the suspensions. These microflocculation phenomena only occur at high ionic strength and appear to be totally absent for ionic strengths $\leq 10^{-3}$ M/L.

For all sizes investigated here, particles are strongly affected by Brownian motion. As already shown,[39] it is then possible to define an effective equivalent hard sphere volume fraction ϕ_{eff} by considering the whole volume trapped by the freely rotating anisotropic platelets. In that case,

$$\phi_{\text{eff}} = \frac{4}{3}\pi N r_{\text{eq}}^{\ 3} \tag{1}$$

where r_{eq} is the equivalent radius of the particles taken as half the average diameter of the particles and N is the number density of particles. Knowing the average length a and width b from TEM measurements and the thickness t being obtained from

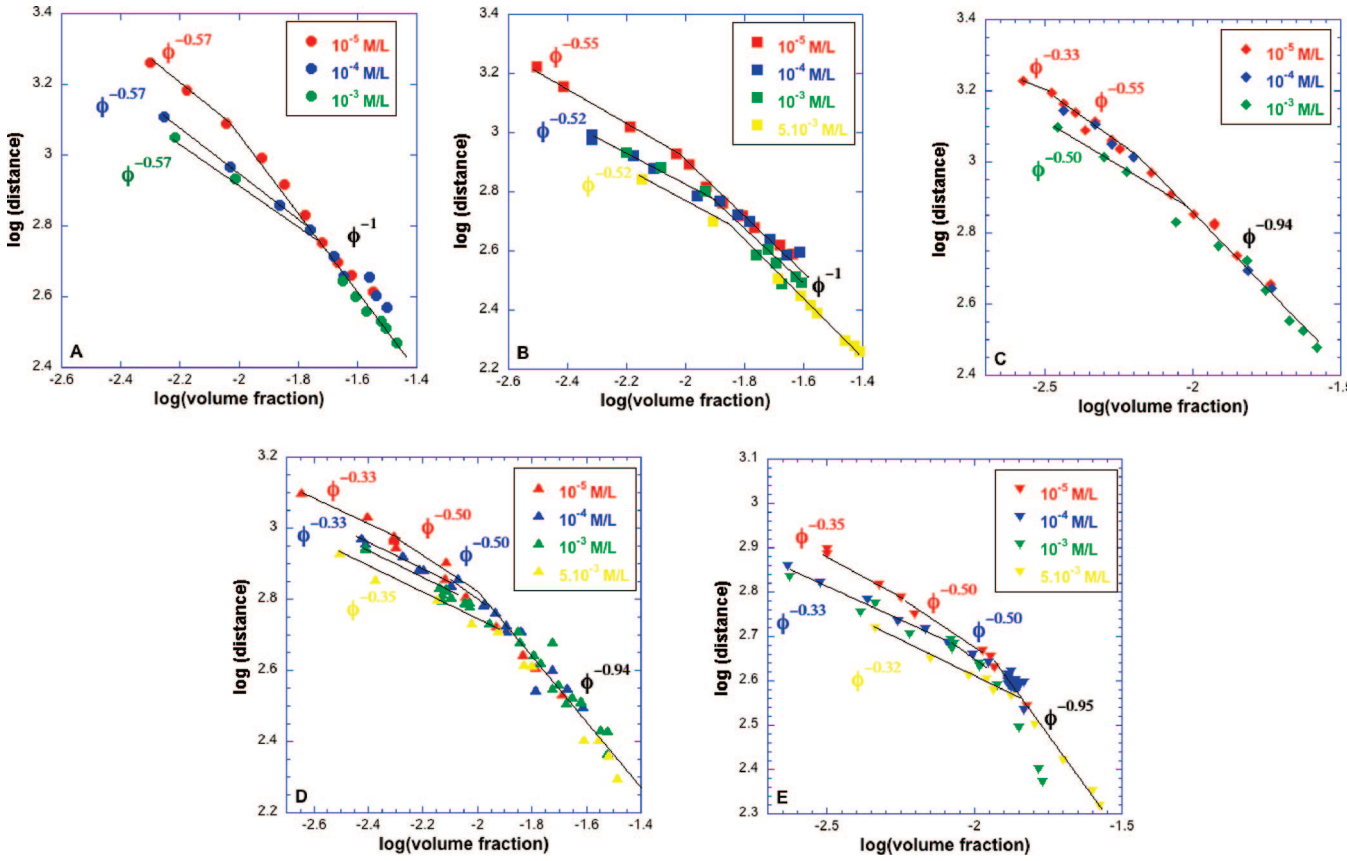

Figure 2. Evolution of the interparticle distances with volume fraction for the five nontronite size fractions: A, S1; B, S2; C, S23; D, S3; E, S4.

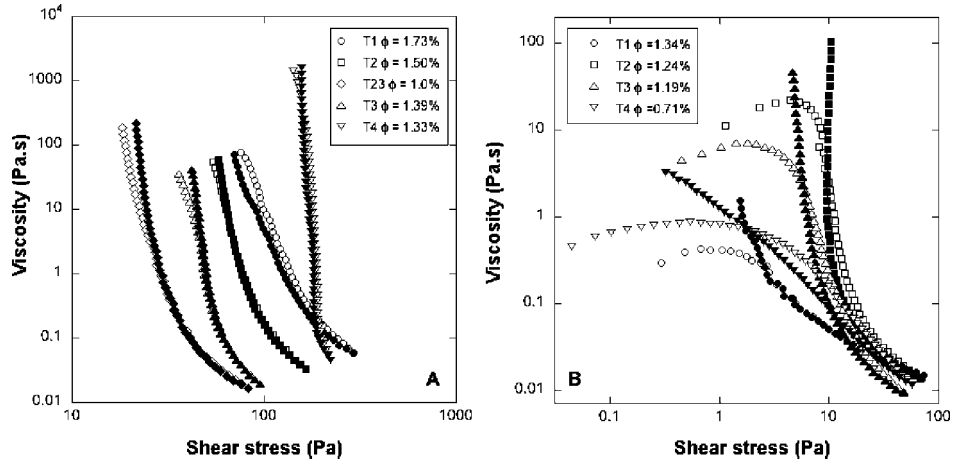

Figure 3. Typical viscosity vs shear stress curves: A, ionic strength 10^{-4} M/L; B, ionic strength 5×10^{-3} M/L.

swelling laws, ϕ_{eff} can then be expressed as a function of the particle volume fraction ϕ as

$$\phi_{\text{eff}} = \frac{4}{3}\pi\left(\frac{a+b}{4}\right)^3 \varphi \frac{1}{abt} \tag{2}$$

Rheological data obtained on nontronites can then be approached in the framework of the extended hard sphere model presented in previous work on clay suspensions.[39] In such a model based on Quemada's approach,[40] the viscosity of interacting disks can be represented using the following equation

$$\eta_r = \frac{\eta_\infty}{\eta_f}\left(\frac{1+Pe}{\chi+Pe}\right)^2 \quad \text{with } \chi = \frac{1-\frac{\alpha\phi_{\text{eff}}}{\phi_0^*}}{1-\frac{\alpha\phi_{\text{eff}}}{\phi_\infty^*}} \tag{3}$$

where η_r is the relative viscosity of the suspension, η_∞ is its viscosity under infinite shear, and η_f is the viscosity of the suspending fluid. *Pe* is a hydrodynamic Peclet number that can

(39) Baravian, C.; Vantelon, D.; Thomas, F. *Langmuir* **2003**, *19*, 8109.
(40) Quemada, D.; Berli, C. *Adv. Colloid Interface Sci.* **2002**, *98*, 51.

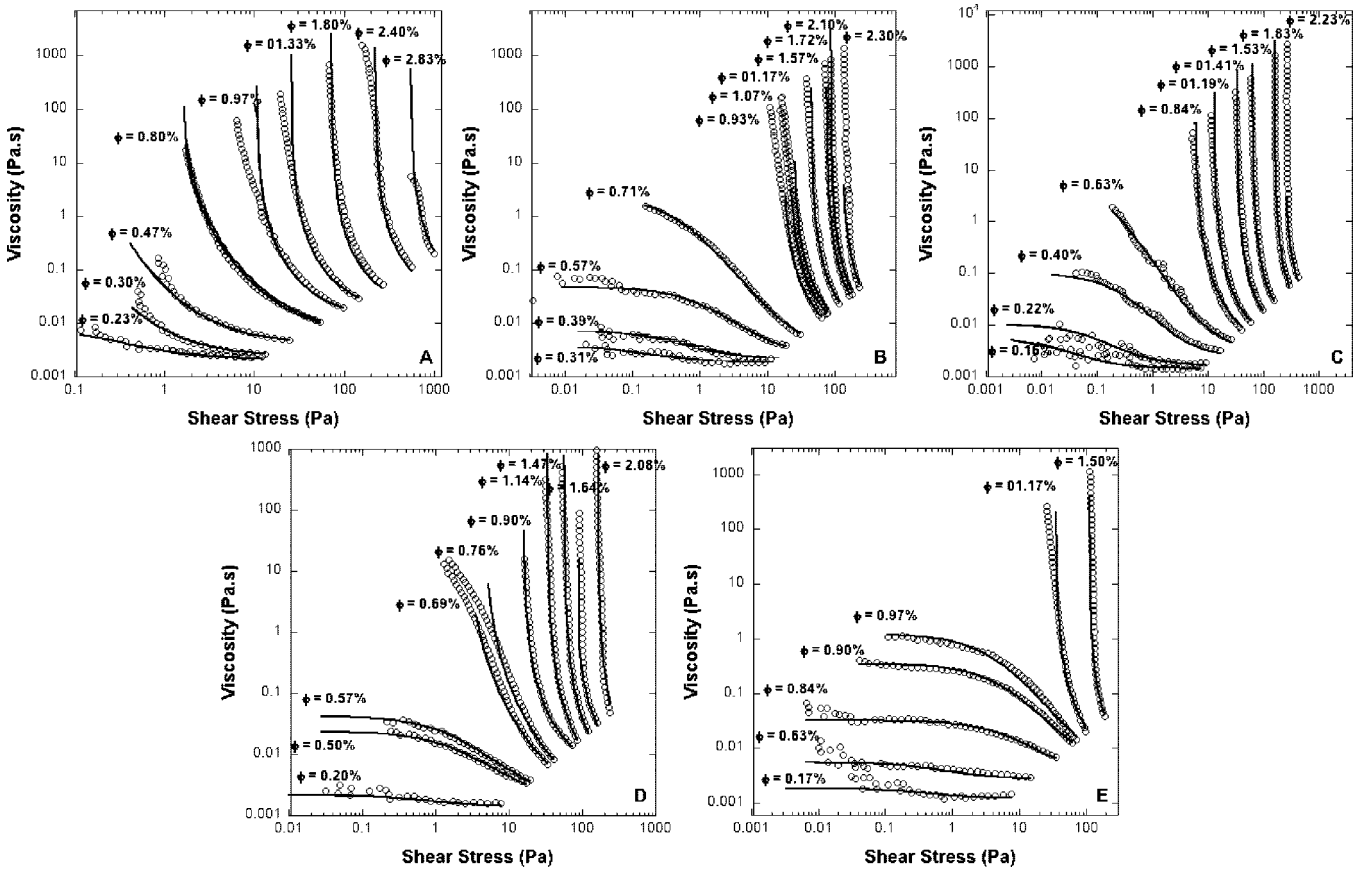

Figure 4. Experimental and modeled flow curves for an ionic strength of 10^{-5}M/L: A, S1; B, S2; C, S23; D, S3; E, S4.

Table 2. Volume Fractions (%) Corresponding to the Sol−Gel Transition of Nontronite Particles Determined from Oscillatory or Flow Measurements for Various Ionic Strengths

		10^{-5} M/L	10^{-4} M/L	10^{-3} M/L	5.10^{-3} M/L
S1	oscillatory	0.7 ± 0.1	1.0 ± 0.1	1.15 ± 0.1	1.03 ± 0.1
	flow	0.7 ± 0.1	1.06 ± 0.1	1.30 ± 0.1	1.20 ± 0.1
S2	oscillatory	0.63 ± 0.1	0.83 ± 0.1	0.95 ± 0.1	0.80 ± 0.1
	flow	0.73 ± 0.1	0.88 ± 0.1	1.10 ± 0.1	0.76 ± 0.1
S23	oscillatory	0.55 ± 0.1	0.65 ± 0.1	0.77 ± 0.1	
	flow	0.60 ± 0.1	0.68 ± 0.1	0.77 ± 0.1	
S3	oscillatory	0.60 ± 0.1	0.078 ± 0.1	0.93 ± 0.1	0.66 ± 0.1
	flow	0.77 ± 0.1	0.83 ± 0.1	1.02 ± 0.1	0.90 ± 0.1
S4	oscillatory	0.90 ± 0.1	1.09 ± 0.1	1.24 ± 0.1	0.85 ± 0.1
	flow	0.99 ± 0.1	1.3 ± 0.1	1.19 ± 0.1	0.73 ± 0.1

be evaluated as $Pe \approx \sigma r_{eq}^3/E \equiv \sigma/\sigma_C$ that compares the hydrodynamic energy with Brownian and interaction energies E. In such a framework, σ_C is a critical shear stress that is reached when hydrodynamic effects are comparable to the other energies in the system, i.e. Brownian motion and interaction energy. The parameter α adjusts the value of ϕ_{eff} by taking into account the possible orientation of the particles. It is then equal to 1 before any orientational effects occur in the system and reaches a value of r_{eq}/t for fully oriented platelets. Finally, ϕ_0* and ϕ_∞* are defined as critical effective volume fractions at rest and under infinite shear.[40] For a suspension exhibiting a yield stress at rest, χ becomes negative, and in that case, the yield stress $\sigma_y = -\chi\sigma_C$. If the viscosity remains finite at zero shear, then $\chi = (\eta_\infty/\eta_0)^{1/2}$. Using such a model, the experimental viscosity vs shear stress curves can be fitted using three parameters, η_∞, χ, and σ_C.

As an illustration, Figure 4 presents the results of such a procedure applied for an ionic strength of 10^{-5} M/L for the five size fractions of nontronite particles. For clarity reasons, all the volume fractions used in the study are not presented in this figure. Most experimental shear stress vs viscosity curves can be satisfactorily reproduced using the proposed rheological model. Two remarks must however be made. (i) Curves displaying a S-shape and a high viscosity such as those obtained for S3 particles at volume fractions around 0.7% are not properly reproduced (Figure 4D). This is certainly due to the use of three fitting parameters only, but in order to properly compare all the curves, we chose not to use any additional fitting parameter. (ii) For the smallest particles, even at a shear rate of 5000 s^{-1}, no inflection of the viscosity is observed for intermediate volume fractions (Figure 4E), and in such a case, the determination of η_∞ is not possible.

Sol−Gel Transition. The use of such a model provides an alternative way to determine the sol−gel transition, based on the change of sign of the parameter χ, whereas the method used in part 1 of this series of papers[32] was based on oscillatory measurements, the gel state being defined for $G' > G''$ and $G' \geq 1$ Pa. Table 2 presents a comparison between the volume fractions in percent corresponding to the sol−gel transition,

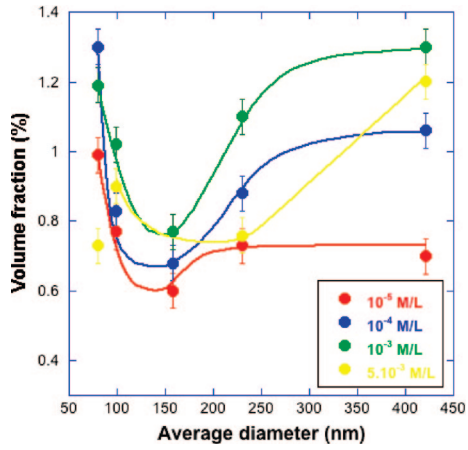

Figure 5. Evolution with average particle size of the volume fraction corresponding to the sol−gel transition of nontronite particles at various ionic strengths.

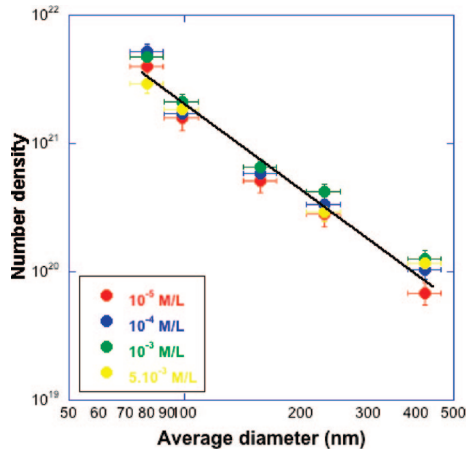

Figure 6. Evolution with average particle size of the number density corresponding to the sol−gel transition of nontronite particles at various ionic strengths. The solid line corresponds to a power law with an exponent of −2.

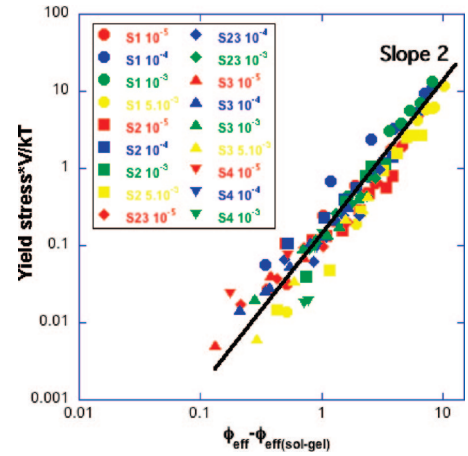

Figure 7. Evolution of the normalized yield stress of nontronite suspensions as a function of the reduced effective volume fraction.

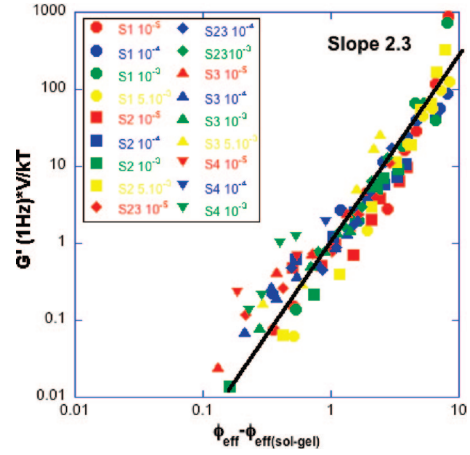

Figure 8. Evolution of the normalized elastic modulus of nontronite suspensions as a function of the reduced effective volume fraction.

determined using both methods. In most cases, the values deduced from the treatment of the flow curves are slightly higher than those determined from the oscillatory measurements. In the case of nontronites, such a discrepancy might be due to the fact that the nematic phase can display a significant elasticity, due to long-range interaction, which in turn may lead to a slight underestimation of the true volume fraction corresponding to the sol−gel transition when it is measured before preshear in oscillatory measurements.

Using the data obtained from Table 2, it is possible to plot the evolution of the volume fraction corresponding to the sol−gel transition (defined on the basis of flow measurements) as a function of particle size (Figure 5). It appears that for the small sizes the volume fractions corresponding to the sol−gel transition decrease with increasing size, whereas the tendency is reversed for higher sizes. It must be pointed out that in our previous study of the sol−gel transition of Wyoming montmorillonite,[22] an increasing linear relationship was found between the volume fraction and particle size. However, as only three sizes were investigated, the reversal of tendency was not observed, but it may well have been present. In any case, such an evolution cannot be interpreted in simple terms.

In order to reach a better insight into the dependence of the sol−gel transition as a function of particle size, it is actually more relevant to plot the same curves as a function of the number density of particles, which takes into account the morphological information derived from TEM and SAXS experiments (Figure 6). The number density at the sol−gel transition appears to evolve as the inverse square of the average diameter. Such an evolution suggests that the objects that are at the origin of the sol−gel transition might not be individual particles but stacks of particles stabilized by ionic repulsions, an explanation that was also proposed in the case of Wyoming montmorillonite.[22]

Yield Stress and Elasticity. As far as the mechanical properties of the gel are concerned, the rheological modeling carried out allows determining the yield stress of the nontronite suspensions. Figure 7 presents the evolution of yield stress as a function of a reduced effective volume fraction defined as the effective volume fraction minus a critical effective volume fraction, corresponding to the sol−gel transition (Table 2). In order to normalize the results for all sizes, the yield stress is multiplied by the volume of the particles, and divided by kT in order to obtain an a dimensional number. It appears that the measurements for all the samples fall on the same master curve and that the normalized yield stress varies as a function of the reduced effective volume fraction to the power 2. As shown in numerous publications (e.g., refs 28, 41−43) and recently rationalized[44] in

(41) Tadros, Th. F. *Adv. Colloid Interface Sci.* **1996**, *68*, 97.
(42) Michaels, A. S.; Bolger, J. C. *Ind. Eng. Chem. Fundam.* **1962**, *1*, 153.

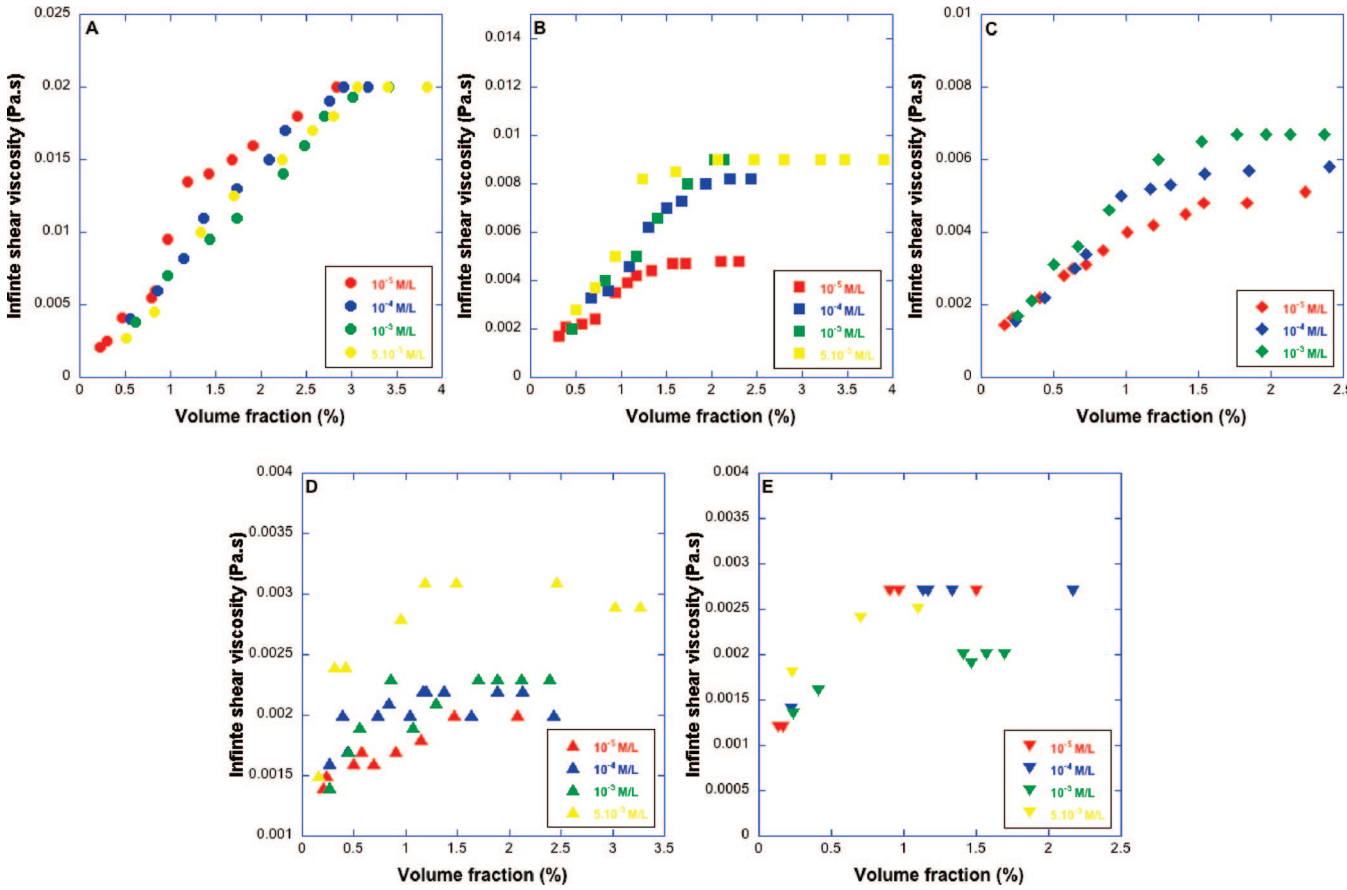

Figure 9. Evolution of the infinite shear viscosity with volume fraction: A, S1; B, S2; C, S23; D, S3; E, S4.

the case of the phase transitions of attractive colloidal systems (glass transition, gelation, or aggregation), the exponent of such relationship is close to 3.4, i.e., significantly larger than the value observed for nontronite. This may suggest that the behavior of nontronite is not controlled by attractive interactions between particles. Furthermore, in attractive gels, the size of the scaling exponent is very sensitive to the strength of the attraction between particles. In the case of nontronite, it appears that there is nearly no dependence of the scaling exponent with salt concentration, indicating that within that regime, attractive interactions likely do not play a significant role.

Figure 8 presents the evolution of the normalized elastic moduli G' using the same normalization as that carried out for the yield stress. As in the case of yield stress, such a treatment leads to a single master curve that exhibits a $(\phi - \phi_c)^{2.3}$ dependence. The data points are more scattered at both ends of the curve, i.e. for low and high volume fractions. At low volume fractions, the abscissas are extremely sensitive to the determination of the critical effective volume fraction, which is obviously not perfectly accurate. At high volume fractions, some of the gels, especially for the large size particles, are extremely stiff and the exact determination of G', with the very small cone-plate geometry used in the present study, is then less accurate. In any case, the exponent obtained is significantly lower than the predicted value of 4 for attractive systems.[44] Once again no dependence of ionic strength is observed (though the data for an ionic strength of 5×10^{-3} M/L may be fitted with a slightly higher exponent), confirming the absence of significant attractive interactions in the system.

Furthermore, in their study on laponite; Mourchid et al.[25] applied the same treatment to analyze the evolution of G' as a function of reduced concentration $(c - c_{sol-gel})$ and found that all the curves could be described whatever the ionic strength with an exponent of 2.35, i.e., the same value as that found in the present study on nontronite, whereas values around 2.5 were obtained for Wyoming montmorillonite.[22] In addition, the analysis carried out by Callahan and Ottewill[14] on the evolution of G' as a function of concentration also revealed a similar power law dependence. It then appears that such a behavior might be characteristic of all swelling clay minerals, whether they present an isotropic/nematic transition before the sol−gel transition or not. To support such an assumption, it is worth recalling that, as far as the local lamellar structure of the gel is concerned, all the natural swelling clay minerals that we have investigated by SAXS display similar features.[31] It then appears that the existence of an isotropic/nematic transition before the sol/gel transition does not lead to differences in the gel mechanical properties.

Infinite Shear Viscosity. The evolution of the infinite shear viscosity as a function of volume fraction for the five nontronite size fractions shows similar trends, whatever the size (Figure 9). The infinite shear viscosity increases with increasing volume fraction before reaching a pseudoplateau, the position and amplitude of which depend on ionic strength and average size. This pseudoplateau reveals the orientation of the particles. Indeed, in the range of volume fractions studied here, the viscosity of particles oriented by hydrodynamic forces depends only marginally on the number of platelets actually present in the flow.

(43) Saint-Michel, F.; Pignon, F.; Magnin, A. *J. Colloid Interface Sci.* **2003**, *267*, 314.
(44) Trappe, V; Prasad, V.; Cipelletti, L.; Segré, P. N.; Weitz, D. A. *Nature* **2001**, *411*, 772.

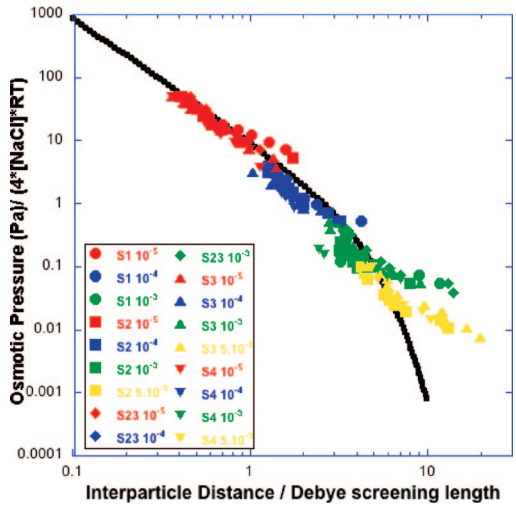

Figure 10. Evolution of the reduced osmotic pressure as a function of interparticle distance for nontronite particles. The thick black line corresponds to the asymptotic solution calculated from equation (A6).

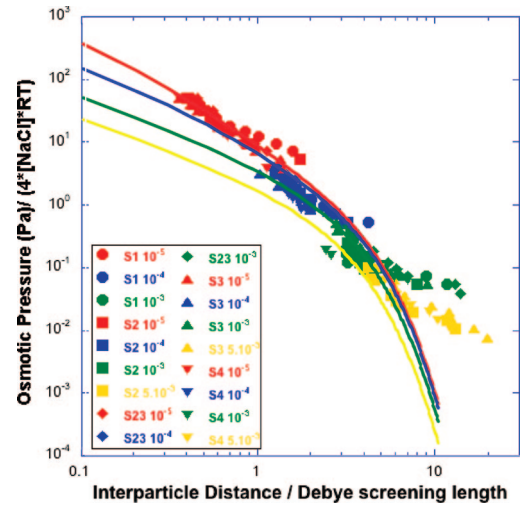

Figure 11. Evolution of the reduced osmotic pressure as a function of interparticle distance for nontronite particles. The solid lines correspond to the osmotic pressure calculated from the Poisson−Boltzmann theory applied to charged infinite parallel plates assuming an effective charge of the particles of −0.01 C/m^2: red, 10^{-5} M/L; blue, 10^{-4} M/L; green, 10^{-3} M/L; yellow, 5×10^{-3} M/L.

Discussion

Ionic Repulsions. As previously shown, some of the rheological properties of swelling clay gels can be understood on the basis of ionic repulsions between charged plates.[45] However, as the distance between the charged platelets was not known in that previous study, the treatment was based on a simple DLVO theory with a correction factor to reproduce the experimental data. In the case of nontronite, as the interparticle distances derived from the analysis of the SAXS patterns (Figure 2) are known in the whole phase diagram, it is possible to clearly assess the role of ionic repulsions by calculating the osmotic pressure (assuming infinite parallel charged plates) and comparing the values thus obtained with the experimental ones.

The nominal charge of the nontronite used here can be calculated from the unit cell dimensions of the basal surface (i.e., around 50 Å^2) and the amount of compensating cations 0.72 per unit cell). Then we have for the nontronite charge $C = 0.72 \times (-1.602 \times 10^{-19})/100 \times 10^{-20} = -0.11$ C/m^2. For this charge value of −0.11 C/m^2, as shown in the Appendix, the Poisson−Boltzmann (PB) equation can be solved analytically for a symmetrical 1:1 electrolyte for the case of two parallel infinite plates in the case of half-separation distances between plates ≫0.32 nm, which is the case encountered in the present study.[46,47] As shown in Figure 10, the agreement between experiment and theory based on eq A6 is very satisfactory.

However, in the case of charged clay minerals, various measurements, simulation work, and theoretical descriptions[32,48−50] have shown that the effective charge of the particles in suspensions is much lower than the structural charge. It is then interesting to compare the experimental and calculated values of osmotic pressure for a lower charge such as −0.01 C/m^2. In that case, eq A6 cannot be used any longer and a full numerical resolution of the PB equation for infinite charged planes must then be carried out (Figure 11).

The agreement between calculated and experimental osmotic pressures is in that case slightly better, especially for ionic strengths of 10^{-4} and 10^{-3} M/L. However, considering the data, it would be difficult to determine accurately the effective charge on the basis of this analysis based on osmotic pressure measurements. It would certainly be interesting in that context to try to obtain more concentrated dispersions, which should provide a better sensitivity to the actual value of the effective charge.

The treatment based on the PB equation also reveals that data obtained at relatively high ionic strength (especially for 5×10^{-3} M/L) display a systematic discrepancy between experimental and calculated values, experimental values being systematically higher than the calculated ones. In this range of ionic strength, as already discussed, microflocculation phenomena seem to occur and the local order between platelets can then be significantly perturbed. Indirect evidence for this disorder can be obtained by comparing, for similar volume fractions and increasing ionic strength, the SAXS patterns of nontronite of S2, S3, and S4 (Figure 12). It clearly appears that the correlation peaks are systematically much broader for the highest ionic strength used, i.e. 5×10^{-3} M/L. It must be pointed out that in the case of the highest size fraction of nontronite, no correlation peaks indicative of interparticle distances were observed for an ionic strength of 5×10^{-3} M/L, which suggests that the local order is even more disturbed for the large size particles.

Excluded Volume Effects. The excluded volume contribution depends on the orientational order of the particles and must be considered differently in two distinct domains: the isotropic state at low volume fraction, where the particle orientation is fully random, and the nematic state at high volume fraction, where particles display long-range order. The separation between these two domains corresponds to a critical effective volume fraction, ϕ_{eff}*, whose position is higher than that corresponding to the rotation limitation (isotropic−nematic transition) given by the random packing fraction of the spheres constructed around the particles ($\phi_{\text{eff}} = 0.64$ for monodisperse spheres). The fact that the value of 0.64 roughly corresponds to the isotropic/nematic transition can be evidenced in Figure 13, which compares the number density of particles at the isotropic binodal of the I/N transition[32] with that calculated for $\phi_{\text{eff}} = 0.64$.

(45) Saikari, N.; Kobayashi, M.; Adacgi, Y. *J. Colloid Interface Sci.* **2005**, *283*, 245.
(46) Derjaguin, B. V.; Churaev, N. V.; Muller, V. M. *Surface Forces*; Plenum Press: New York, 1987 p 281.
(47) Moyne, C.; Murad, M. A. *Transport Porous Media* **2006**, *63*, 13.
(48) Durand-Vidal, S.; Turq, P.; Marang, L.; Pagnoux, C; Rosenholm, J. B. *Colloids Surf. A* **2005**, *267*, 117.
(49) Meyer, S.; Levitz, P.; Delville, A. *J. Phys. Chem. B* **2001**, *105*, 10689.
(50) Trizac, E.; Bocquet, L.; Agra, R.; Weiss, J.-J.; Aubouy, M. *J. Phys.: Condens. Matter* **2002**, *14*, 9339.

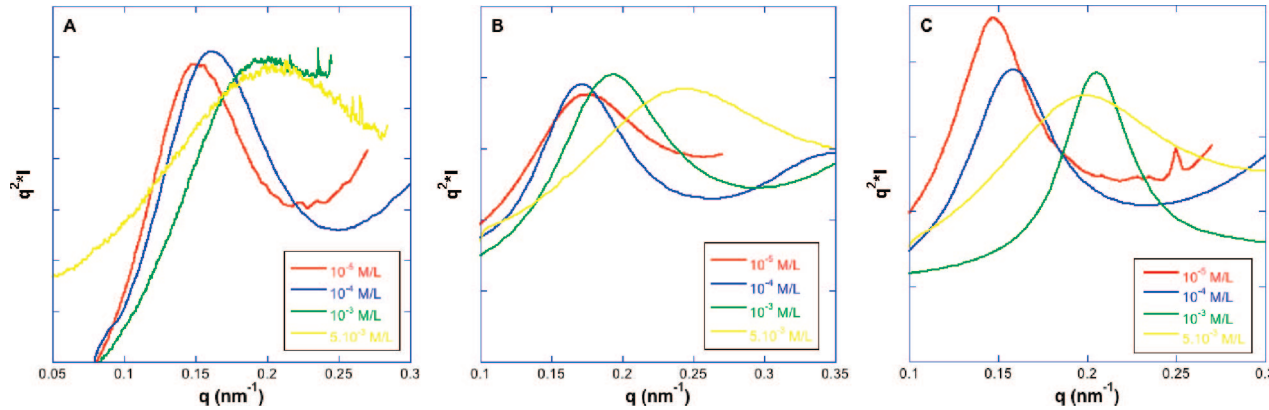

Figure 12. Evolution with ionic strength (IS) of the product $q^2I(q)$ as a function of q for nontronite suspensions: (A) S2, IS 10^{-5} M/L, ϕ 2.1%; IS 10^{-4} M/L, ϕ 2.2%; IS 10^{-3} M/L, ϕ 2.13%; IS 5.10^{-3} M/L, ϕ 2.07%. (B) S3, IS 10^{-5} M/L, ϕ 2.07%; IS 10^{-4} M/L, ϕ 2.13%; IS 10^{-3} M/L, ϕ 2.13%; IS 5.10^{-3} M/L, ϕ 2.43%. (C) S4, IS 10^{-5} M/L, ϕ 1.20%; IS 10^{-4} M/L, ϕ 1.47%; IS 10^{-3} M/L, ϕ 1.58%; IS 5.10^{-3} M/L, ϕ 1.59%.

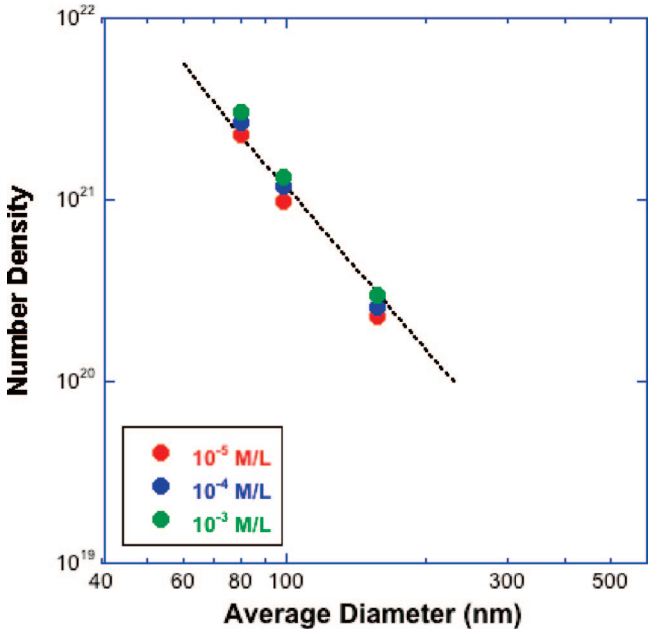

Figure 13. Comparison between the experimental isotropic binodal of the I/N transition with that calculated assuming a value of 0.64 (random packing fraction for spheres).

Below 0.64, the particles are free to rotate and the average interparticular distance is then given by $\bar{D}/2r_{eq} = (\phi_{eff}^*/\phi_{eff})^{1/3}$ where $\bar{D}$ is the average interparticular distance and r_{eq} is the average particle radius. When the volume fraction increases, the spheres encompassed by the rotating the particles are significantly interpenetrated (Figure 14). The geometrical configuration of the particles can then be seen as a packing of oblate ellipsoids with a length $2r_{eq}$ and a thickness that depends on the space left between the particles, i.e. the average interparticular distance $\bar{D}$. For high enough volume fractions, the oblate ellipsoid thickness can be estimated as the interparticle distance, leading to $\bar{D}/2r_{eq} = \phi_{eff}^*/\phi_{eff}$.

These two different interparticle distance limits for low and high volume fractions can be linked by an harmonic average: $2r_{eq}/\bar{D} = (\phi_{eff}/\phi_{eff}^*)^{1/3} + (\phi_{eff}/\phi_{eff}^*)$ which recovers both asymptotic limits.

In order to compare all sizes and ionic strengths, the evolution of the ratio of the interparticle distance to the average radius can be plotted as a function of the effective volume fraction (Figure 15). Using this rescaling, all the data, whatever the particle size

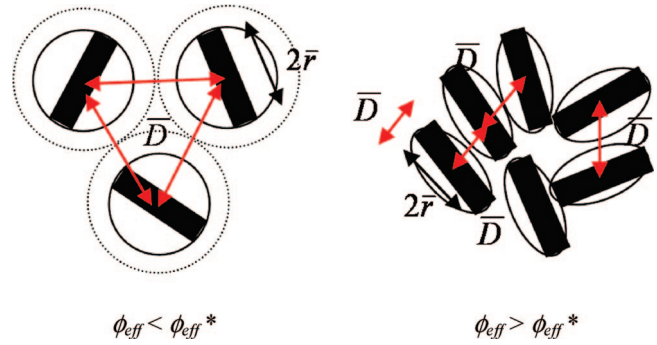

Figure 14. Schematic representation of the effective critical volume fraction. The size and thickness of the particles are not to scale.

and ionic strength, fall on the same master curve. Furthermore, using a value of ϕ_{eff}^* of 1, an excellent agreement between the model and experiment is obtained.

For high effective volume fractions, all curves lie close together, which shows that excluded volume effects dominate in this region of the curves. In the transition region and at low effective volume fraction, both size and ionic strength affect these curves (Figure 2), and the fine details are not fully reproduced by the model. Still, the discrepancy between model and experiments remains rather limited, revealing that excluded volume effects also play an important role in these regions of the phase diagrams.

High Shear Flow Properties. This section is devoted to the discussion of the infinite shear viscosity and to the information it provides in terms of particle orientation under flow. Figure 16 presents the data of Figure 10 replotted as a function of effective volume fraction together with the evolution of infinite shear viscosity for hard spheres according to $\eta_\infty = \eta_f(1 - \phi_{eff}/\phi_\infty^*)^{-2}$, where ϕ_∞^* is the random close packing fraction taken as 0.71.[51] All curves gather together, which shows again that excluded volume contributions play a significant role under high shear flow.

Except in the case of the smallest particles at an ionic strength of 5×10^{-3} M/L, i.e. when flocculation phenomena are the most operative, none of the data fall on the hard sphere behavior, which shows that, even at very low volume fractions, particle alignment plays a role in the viscosity of the suspension. A different conclusion was reached on a previous study on montmorillonites.[41] However, in this case, particle size was an

(51) Russell, W. B.; Saville, D. A., Schowalter, W. R. *Colloidal Dispersions*, 2nd ed.; Cambridge University Press, Cambridge UK, 1991.

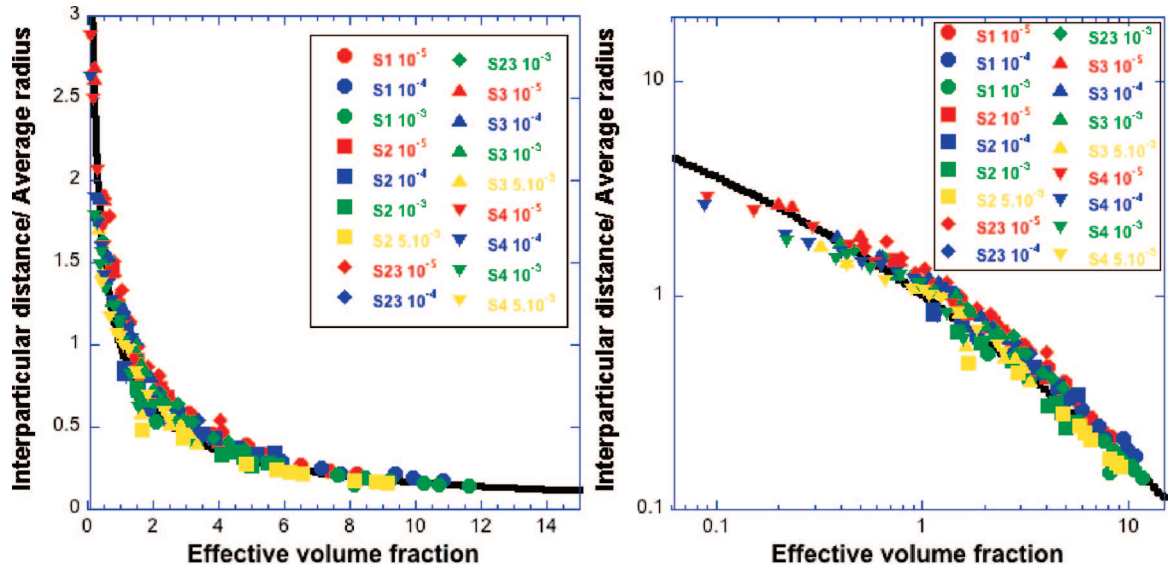

Figure 15. Evolution of the ratio interparticular distance/average radius as a function of effective volume fraction.

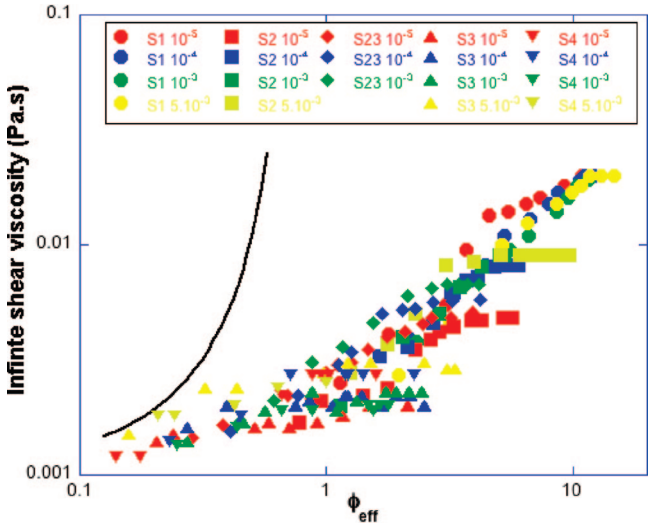

Figure 16. Evolution of the infinite shear viscosity as a function of effective volume fraction. The black line corresponds to the evolution of the infinite shear viscosity for hard spheres.

adjustable parameter, whereas, in our case, the particle sizes were actually measured.

Furthermore, in this range of volume fraction, the viscosity may be affected by the electroviscous effect and could then be overestimated. The existence of an electroviscous effect for dilute suspensions of Na montmorillonite was indeed evidenced in a recent paper.[52] In order to check for the existence of such an effect, it is possible, using data points for effective volume fractions <1, to determine the intrinsic viscosity $[\eta]$ defined as $\lim_{\phi\to 0}\eta_{inh}$, where η_{inh}, the inherent viscosity, is defined as $\ln(\eta/\eta_f)/\phi$.[53] Figure 17A displays the evolution of $[\eta]$ as a function of the Debye length for the five nontronite size fractions. A linear increase of $[\eta]$ can be observed, revealing the presence of an electroviscous effect. The values of $[\eta]$ and their evolution with κ^{-1} are similar to those determined previously for montmorillonite suspensions.[52] Due to the limited number of data points in the low volume fraction region, it is difficult to distinguish between the primary and secondary electroviscous effects.

In order to take into account the size dependence of the electroviscous effect, the intrinsic viscosity was calculated using the effective volume fraction instead of the true particle volume fraction. As shown in Figure 17B, in that case all data points gather on the same curve where $[\eta]$ depends on the product of κ by the average diameter of the particles.

The fact that electroviscous effects are present and increase somehow the viscosity reinforces the statement that, even at very low effective volume fractions, orientational effects play a significant role in the viscosity of nontronite suspensions. In the range of higher volume fractions, it appears more relevant to compare the infinite shear viscosity with that calculated on the basis of ellipsoids oriented along the flow rather than spheres (Figure 14). In that case, as $\eta_s/\eta_f = (1 - \phi/\phi^*)^{-2}$, if one replaces ϕ by its value for ellipsoids, it comes

$$\frac{\eta_s}{\eta_f} = \left(1 - \frac{\phi_{ellipsoids}}{\phi^*}\right)^{-2} = \left(1 - \frac{\phi_{eff}\dfrac{\bar{D}}{2r_{eq}}}{\phi^*}\right)^{-2} \cong \left(1 - \frac{\phi_{eff}}{\dfrac{\left(\dfrac{\phi_{eff}}{\phi^*}\right) + \left(\dfrac{\phi_{eff}}{\phi^*}\right)^{1/3}}{\phi^*}}\right)^{-2} \quad (4)$$

For $\phi^* \cong 1$, this expression simplifies as $\eta_s/\eta_f \cong [\phi_{eff}{}^{-2/3}/(1 + \phi_{eff}{}^{-2/3})]^{-2} = (1 + \phi_{eff}{}^{2/3})^2$.

Figure 18 presents the comparison between the experimental values of the infinite shear viscosity and those calculated according to eq 4 with a value of ϕ^* of 1. It appears that the general trend is well-described. The data points deviate from the ellipsoid behavior to reach pseudoplateaus of viscosity at ϕ_{eff} and viscosity values that depend on both size and ionic strength. Both values clearly decrease with decreasing particle size (Figures 16 and 18). The size dependence of these two features is linear (Figure 19). This shows that the smaller the particles, the easier and better their orientation in the shear flow, which is far from being intuitive. These two graphs also reveal an ionic strength dependence: the lower the ionic strength, the better the orientation, which may be linked to a better orientation at lower ionic strength, a feature that was suggested by the better orientational order

(52) Adachi, Y.; Nakaishi, K.; Tamaki, M. *J. Colloid Interface Sci.* **1998**, *198*, 100.

(53) Hiemenz, P. C.; Rajagopalan, R. *Principles of Colloid and Surface Chemistry*, 3rd ed.; Marcel Dekker Inc.: New York, 1997.

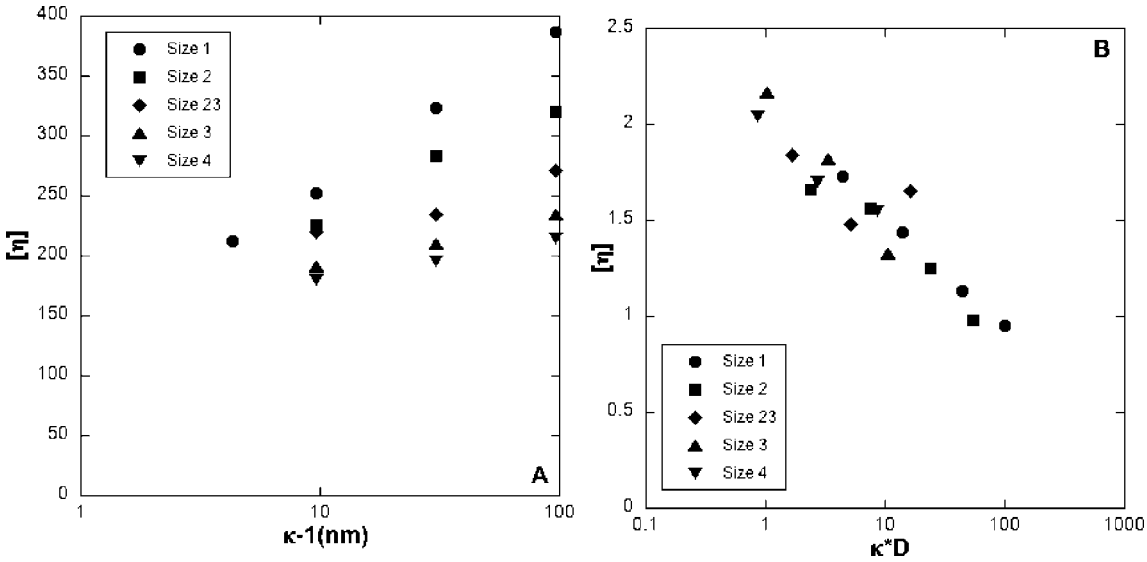

Figure 17. (A) Evolution of the intrinsic viscosity as a function of Debye length for the five size fractions of nontronite. (B) Evolution of the normalized intrinsic viscosity as a function of the product of the inverse Debye length by the average diameter of the particles.

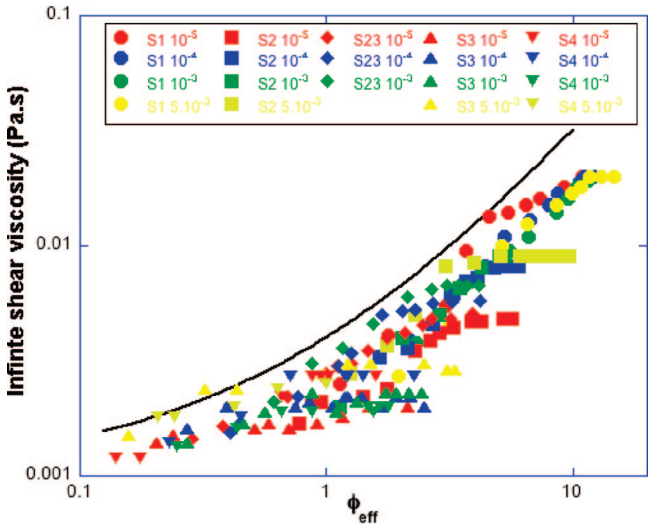

Figure 18. Evolution of the infinite shear viscosity as a function of effective volume fraction. The black line corresponds to the evolution of the infinite shear viscosity for ellipsoids assuming an effective critical volume fraction of 1.0.

displayed at low ionic strength (Figure 12). In any case, it seems that the particles aligning at high shear flow and controlling the infinite shear viscosity may not be individual particles but rather stacks of particles stabilized in their face to face configuration at distances related to the repulsive interactions between electrical double layers. This conclusion agrees with the fact that the sol−gel transition might involve association of particles rather than individual ones.

Conclusions and Perspectives

By working on size-selected natural clay particles, we have explored in detail the phase behavior of charged anisotropic platelets. All the measurements confirm that, for ionic strength $\leq 10^{-3}$M/L, the system is purely repulsive, and in this range of ionic strength, attractive interactions do not play any significant role in the phase behavior of clay systems. Osmotic pressure measurements show that the system can be well-described using a simple Poisson−Boltzmann treatment based on the interaction between charged infinite parallel planes. In the case of nontronite clay, whereas the isotropic/nematic transition and its evolution with particle size are well understood, the status of the sol−gel transition remains partially unclear. Indeed, the dependence on particle size of the sol−gel transition suggests that it may involve association of objects, i.e. stacks of platelets stabilized by ionic repulsions, rather than individual platelets, a conclusion that was already reached in the case of Wyoming montmorillonite.[22] Despite this complexity, once the gels are formed, their mechanical properties both in terms of elasticity and yield stress can be efficiently renormalized using the volume of the particles, thus yielding single master curves applicable to all particle sizes and all ionic strengths. As far as ionic strength is concerned, this is certainly linked to the fact that both elasticity and yield stress actually measure shear properties of oriented particles and are not sensitive to the normal interparticle forces.

For all the particles, both the swelling laws and rheological behavior can be at the first-order well approached on the basis of excluded volume effects only. Still, electrostatic interactions also play a role on the rheological behavior, as illustrated notably by the high shear viscosity data, which is not fully understood at present. The issue of properly analyzing both electrostatic and excluded volume effects in such systems is of prime importance. Indeed, this is certainly the key to understanding why in most swelling clay minerals studied so far, the isotropic/nematic transition is "missed" and somehow masked by the sol−gel transition. In order to support this statement, it is necessary to study other swelling clay minerals using the same approach as that developed in the present series of papers. In particular, the effect of structural charge and its location should be investigated in detail both experimentally and by simulation work, as the interactions between clay platelets of octahedrally substituted clays have been shown to differ in a subtle but significant way from the interactions between tetrahedrally substituted clay platelets.[54] Preliminary investigations[55] reveal indeed that two other clay minerals with tetrahedral substitution (a high charge nontronite and a beidellite) also display a true isotropic/nematic transition.

Additional information could certainly be obtained by investigating in detail the structure of the suspensions subjected to various external fields. As already shown,[31] clay suspensions

(54) Lubetkin, S. D.; Middleton, S. R.; Ottewill, R. H. *Philos. Trans. R. Soc. London* **1984**, *A311*, 353.
(55) Michot, L. J.; Paineau, E.; Baravian, C.; Bihannic, I.; Duval, J. F. L.; Maddi, S.; Baravian, C.; Levitz, P.; Davidson, P. Manuscripts in preparation.

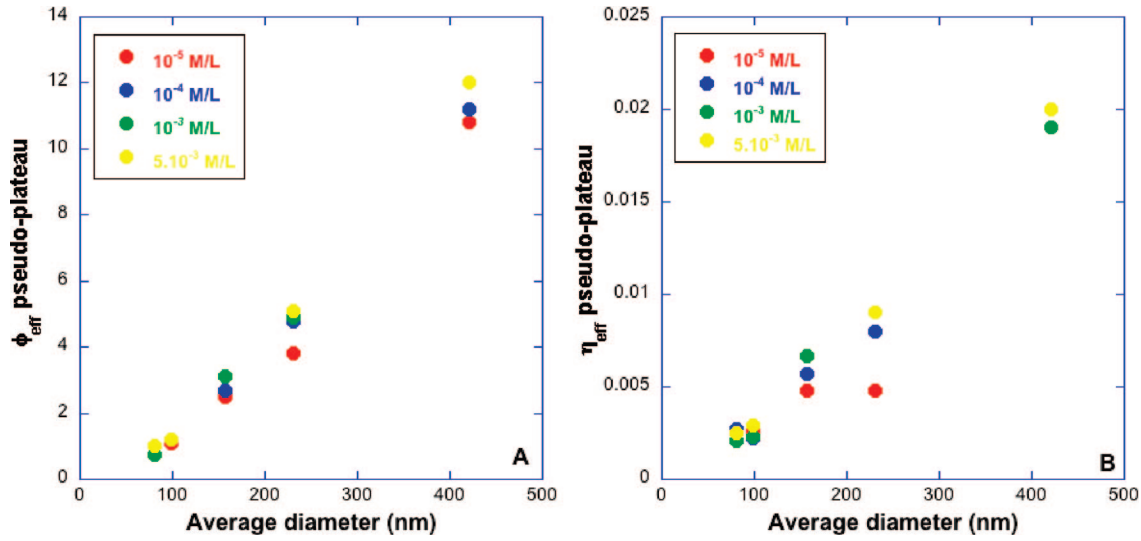

Figure 19. Evolution of the position (A) and value (B) of the pseudoplateau of infinite shear viscosity as a function of the hydrodynamic diameter of the particles.

can be oriented in magnetic fields and should also be sensitive to electrical fields. As far as hydrodynamics are concerned, it would certainly be fruitful to couple structural measurements using scattering experiments with rheological experiments, to analyze in details the orientation of the particles in the flow. Finally, all the rheological experiments carried out in the present study are based on the use of shear flows. It would certainly be relevant to study other flow types such as elongational flows and combined elongational and shear flows in pipes.

Acknowledgment. Support of beamtime at Hasylab by the European Community-Research Infrastructure Action under the FP6 "Structuring the European Research Area" Programme (through the Integrated Infrastructure Initiative "Integrating Activity on Synchrotron and Free Electron Laser Science") Contract RII3-CT-2004-506008 is gratefully acknowledged. We would like to thank Sergio S. Funari and Stefan Roth for their help during the SAXS experiments on beamlines A2 and BW4.

Appendix

For parallel infinite planes with a given surface charge σ, the reduced osmotic pressure reads $\Pi^* = \Pi_{osm}/4c_bRT$, with c_b being the bulk concentration. Π^* is then given by[46,47]

$$\Pi^* = \cot^2 \alpha = \frac{1}{\sin^2 \alpha} - 1 \qquad \text{(A1)}$$

with $H/L_D = \sin \alpha\, G(\varphi,\alpha)$ and $\tan \varphi = \tan \alpha\, |\sigma|/4Fc_b = L_D$ ($0 \le \varphi \le \pi/2$), where $G(\varphi,\alpha)$ is an elliptic integral of the first kind with modulus $\sin \alpha$ and amplitude φ, H is the half-space between the plates, and L_D is the Debye length.

We examine the case where, $\varphi \to \pi/2$ or $\varphi = \pi/2 - \xi$ with $\xi \ll 1$. Under such conditions, we obtain

$$\frac{H}{L_D} = \int_0^{\frac{\pi}{2}} \frac{\sin \alpha\, d\theta}{\sqrt{1 - \sin^2 \alpha \sin^2 \theta}} - \int_{\frac{\pi}{2}-\xi}^{\frac{\pi}{2}} \frac{\sin \alpha\, d\theta}{\sqrt{1 - \sin^2 \alpha \sin^2 \theta}} = \sin \alpha K(\sin^2 \alpha) - E \qquad \text{(A2)}$$

where K is the complete elliptic integral of the first kind. The error function E is given by

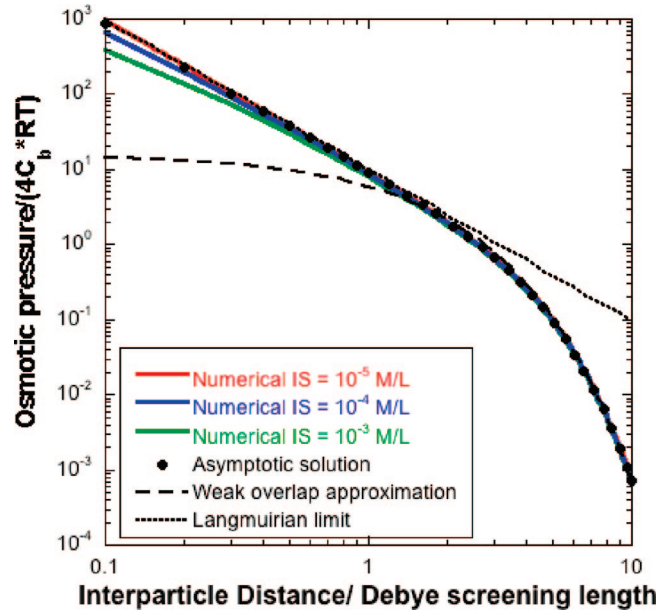

Figure 20. Evolution of the reduced osmotic pressure between charged plates (−0.11 C/m^2) as a function of interparticle distance calculated using various models.

$$E = \int_{\frac{\pi}{2}-\xi}^{\frac{\pi}{2}} \frac{\sin \alpha\, d\theta}{\sqrt{1 - \sin^2 \alpha \sin^2 \theta}} \quad \text{with } 0 \le E \le \int_{\frac{\pi}{2}-\xi}^{\frac{\pi}{2}} \tan \alpha\, d\theta = \xi \tan \alpha \le \tan \xi \tan \alpha = \frac{\tan \alpha}{\tan \phi} = \frac{4Fc_bL_D}{|\sigma|} \qquad \text{(A3)}$$

The approximation is therefore correct if $E \ll H/L_D$ or

$$\frac{4Fc_bL_D}{|\sigma|} << \frac{H}{L_D} \Rightarrow H >> \frac{4Fc_bL_D^2}{|\sigma|} = \frac{2\varepsilon\varepsilon_0 RT}{F|\sigma|} \qquad \text{(A4)}$$

For $|\sigma| = 0.11$ C m^{-2}, the approximation will be correct for $H \gg 3.2 \times 10^{-10}$ m.

In this case, eq A2 reduces to

$$H/L_D = \sin\alpha K(\sin^2\alpha) \quad \text{(A5)}$$

The relation between the reduced osmotic pressure Π^* and the half-separation between the plates is then given by

$$\frac{H}{L_D} = \sqrt{\frac{1}{1+\Pi^*}}K\left(\frac{1}{1+\Pi^*}\right) \quad \text{(A6)}$$

Figure 20 compares the results given by the exact solution of the Poisson−Boltzmann equation (for $c_b = 10^{-3}, 10^{-4}, 10^{-5}$ mol L^{-1}), the classical weak overlap solution, and the Langmuir equation. It clearly appears that the Langmuir equation fails at large normalized distances, whereas the classical weak overlap approximation is not adapted at small distances. Only the full numerical resolutions and the asymptotic solution that has no adjustable parameters can be used to properly reproduce the data.

LA801894A